

Probing Electronic Properties of Molecular Engineered Zinc Oxide Nanowires with Photoelectron Spectroscopy

Carlos A. Aguilar,^{†,‡,⊥,♯} Richard Haight,^{¶,*} Anastassios Mavrokefalos,^{‡,⊥} Brian A. Korgel,^{§,⊥} and Shaochen Chen^{‡,⊥,*}

[†]Biomedical Engineering Department, [‡]Mechanical Engineering Department, [§]Chemical Engineering Department, and [⊥]Center for Nano and Molecular Science and Technology, University of Texas at Austin, Austin, Texas 78712, and [¶]IBM T. J. Watson Research Center, P.O. Box 218, Yorktown Heights, New York 10598. [♯]Present address: MIT Lincoln Laboratory, 244 Wood Street, Lexington, Massachusetts 02127.

ZnO nanowires (NWs) have attracted considerable attention recently, owing to their unique suite of properties that include a large band gap (>3 eV), and optical transparency in the visible regime. ZnO NWs have been leveraged into a myriad of applications from ultraviolet (UV) nanolasers,¹ solar cell anodes,² and photodetectors,^{3,4} to active channels in transparent flexible electronics.⁵ Improving the performance of such technologies will ultimately require measurement and optimization of fundamental electronic properties such as the work function and location of the Fermi level. However, the ability to reproducibly form high-quality contacts to ZnO has remained a significant barrier to electrical assessment of such intrinsic properties. A general optical diagnostic technique that can noninvasively measure such electronic properties on individual ZnO NWs is needed. While experimental approaches such as Rayleigh scattering⁶ and Raman spectroscopy⁷ on isolated carbon nanotubes have been carried out, they do not provide the location of the Fermi level or work function information. Conventional scanning probe techniques such as scanning Kelvin probe microscopy are primarily applicable to planar thin films and versions of scanning tunneling microscopy can provide information on local electronic structure but are limited by the size of the probe tip.⁸

Photoelectron spectroscopy is a particularly powerful experimental method for studying the electronic structure and properties of materials; and when carried out with low energy photons focused onto individual NWs, important new information about sur-

ABSTRACT ZnO nanowires (NWs) are emerging as key elements for new lasing, photovoltaic and sensing applications but elucidation of their fundamental electronic properties has been hampered by a dearth of characterization tools capable of probing single nanowires. Herein, ZnO NWs were synthesized in solution and integrated into a low energy photoelectron spectroscopy system, where quantitative optical measurements of the NW work function and Fermi level location within the band gap were collected. Next, the NWs were decorated with several dipolar self-assembled monolayers (SAMs) and control over the electronic properties is demonstrated, yielding a completely tunable hybrid electronic material. Using this new metrology approach, a host of other extraordinary interfacial phenomena could be explored on nanowires such as spatial dopant profiling or heterostructures.

KEYWORDS: nanowires · zinc oxide · photoelectron spectroscopy · work function · fermi level · self-assembled monolayers

face and “bulk” NW electronic properties can be gleaned.⁹ In this letter, we use a unique, femtosecond laser-based photoelectron spectroscopy system to measure the work function and Fermi level location within the ZnO NW band gap. We then “engineer” the work function through adsorption of polar self-assembled monolayers (SAMs). The attachment of polar molecules to NW surfaces presents a unique opportunity to both selectively pattern¹⁰ and controllably alter NW electronic properties.¹¹ Our choice of phosphonic acid-based SAMs derives from our ability to modify both the magnitude and direction of their dipole moments; this in turn can induce profound reversible changes to the NW valence band properties.

Figure 1a is a schematic of the photoelectron spectroscopy system. Frequency-quadrupled femtosecond laser light (200 nm, 150 fs) was passed into a UHV chamber where it was focused at normal incidence through a Swartzchild reflective objective (NA = 0.5) onto an individual ZnO NW that was

*Address correspondence to rahaight@us.ibm.com, scchen@mail.utexas.edu.

Received for review July 10, 2009 and accepted September 3, 2009.

Published online September 18, 2009.
10.1021/nn900777k CCC: \$40.75

© 2009 American Chemical Society

suspended over a lithographically patterned Si wafer. The Si substrates were mounted onto a three-dimensional piezoelectric stage inside the UHV chamber and the suspended NWs were directed to the focused laser spot. An electron collecting lens was positioned behind the NW to collect the photoemitted electrons (Figure 1b) and the photoelectrons were analyzed by a hemispherical electrostatic analyzer with 20 meV resolution. Since the NWs extended only partially across the gap (Figure 1c), several spectra were recorded along the length of the NW and averaged.

RESULTS AND DISCUSSION

Initial experiments were carried out on as-grown ZnO NWs. The system Fermi level (E_F) was established *via* emission from a clean Pt film in electrical contact with the sample. A negative bias of 15 V on the sample permitted the identification of the electron emission threshold. Spectra of an individual ZnO NW are shown in Figure 2a. The position of the Fermi level was located at 0 eV binding energy, and the photoelectron emission threshold (E_T) was identified at 1.55 eV. The work function (Φ) can be deduced from E_T *via* eq 1:

$$\Phi = h\nu - E_T \quad (1)$$

and for the NW in Figure 2a, the work function is 4.65 eV. The average Φ taken on 30 different native NWs was 4.7 ± 0.2 eV, approximately 0.5 eV lower than its bulk value. For the range of NW diameters studied (90–200 nm), Φ did not show a dependence on diameter, which was also found for smaller diameter (20–50 nm) Si and Ge NWs.⁹ To guarantee the NW was free from charging, all spectroscopy measurements were conducted at low fluxes to avoid space charge effects. Additionally, since ZnO has a relatively high natural doping level ($5 \times 10^{18}/\text{cm}^3$), surface photovoltage effects can be minimized.^{12,13} The hexagonal faceting of the NW, orientation of the facet/edge relative to the detector, surface variations in stoichiometry, and cleanliness of the surface all may have been responsible for the reduction and variation in Φ . This is not unexpected since edges associated with the faceted surfaces are expected to reduce Φ in a manner similar to that found for stepped or roughened surfaces.¹⁴

Surface defects on intrinsic ZnO such as oxygen vacancies serve as strong binding sites for adsorption of various organic and inorganic molecules. The dangling bonds of adsorbates such as oxygen and water can induce extrinsic surface states that are both spatially and energetically localized and may lie within the band gap or overlap with continuum bulk states.¹⁵ To remove water vapor and other adsorbates (CO_2 , O_2); the substrate was annealed *in situ* at 300 °C for 1 min. Figure 2a displays spectra taken on an individual NW before (green curve) and after annealing (blue curve) in vacuum, and annealing in a dry O_2 ambient (red curve). When the ZnO NW was annealed, a substantial increase in the emission intensity was observed and the spectrum was shifted to lower binding energy. We attribute the increase in intensity to the thermolysis of water and other adsorbates remaining from the solution phase growth of the NW. Adsorbed water on the NW surface can both oxidize zinc interstitials and take up oxygen vacancies, effectively acting like a mask. The spectral shift was ascribed to an increase in oxygen vacancies, which can

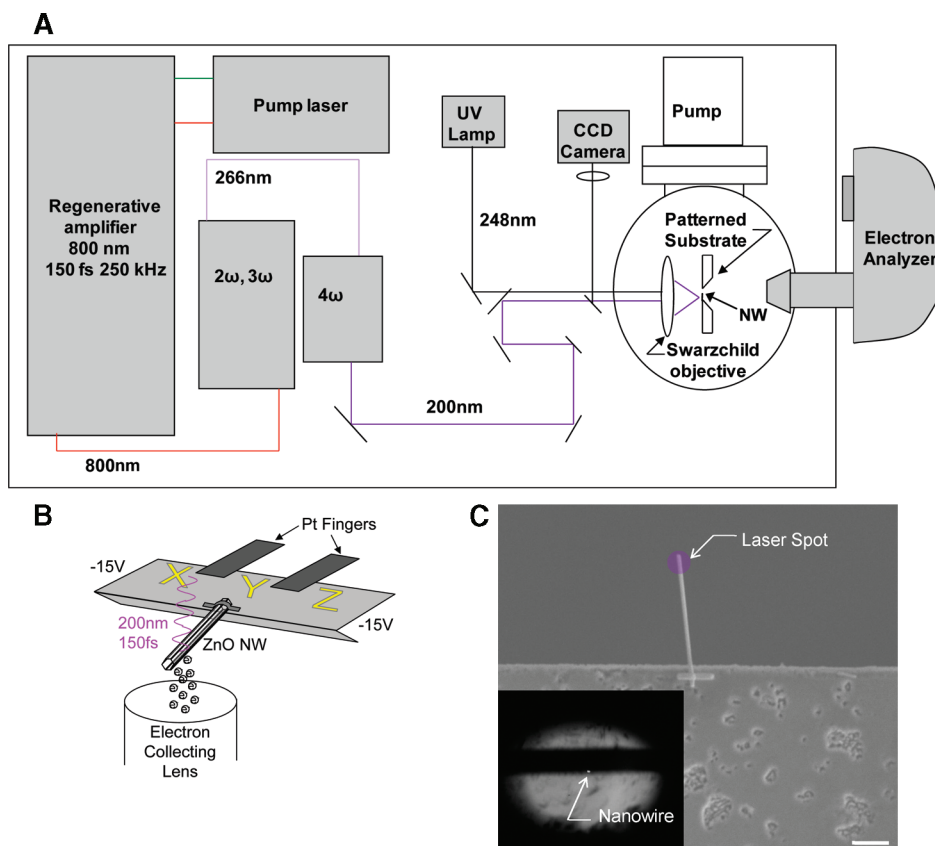


Figure 1. (a) Schematic of low photon energy photoelectron spectroscopy system. Frequency quadrupled femtosecond laser light (150 fs, 200 nm) was sent into an ultrahigh vacuum (UHV) chamber, where it was focused through a Swartzchild objective onto a single nanowire (NW) that was suspended over a slotted wafer. Alphanumeric labels were patterned adjacent to the slots to identify the NW location inside the UHV chamber. (b) Schematic showing single NW photoelectron emission and collection. (c) SEM image of typical NW extending into a patterned slot, where the approximate laser spot size is indicated by a circle. Scale bar is 5 μm . Inset is reflected optical image of NW (bright spot near slot edge) fluorescing under laser irradiation.

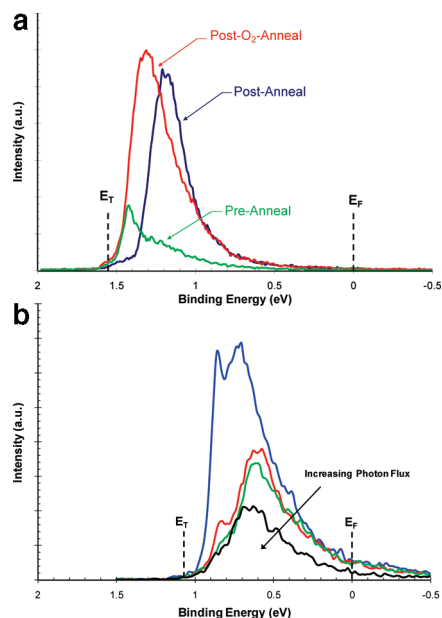


Figure 2. (a) Typical photoelectron spectra from an individual native ZnO NW depicting the emitted electron intensity as a function of binding energy. The green spectrum is from an “as-inserted” ZnO NW while the blue spectrum was collected after annealing the same ZnO NW at 300 °C for 1 min. The valence edge intensity was dramatically enhanced due to thermolysis of water and other electronegative adsorbates. The red spectrum was collected after annealing the same ZnO NW in a partial pressure of oxygen (1×10^{-5} Torr O_2). An energetic shift away from the Fermi level is detected, indicating band bending. (b) Prolonged exposure of ZnO NW to UV light induces a reduction in valence band intensity, indicating photolysis of chemisorbed acceptor ions and band bending. The blue curve is a spectrum of a native NW, and the accumulated photon fluence associated with each spectrum taken thereafter is $7.5e^{22}$ photons/cm² (red curve), $1.5e^{23}$ photons/cm² (green curve) and $2.25e^{23}$ photons/cm² (black curve).

trap free electrons and create a negative surface charge, bending the ZnO valence bands toward the Fermi level. Since the thickness of the depletion layer (L_D), which was determined to be 23 nm for a carrier concentration of 5×10^{18} cm⁻³, is less than the typical NW diameters studied ($D \approx 90\text{--}200$ nm), the shifts we observe in the ZnO spectra can be attributed to changes in the NW work function from band bending.

To confirm this interpretation, the ZnO NWs were annealed at the same temperature in a dry oxygen ambient and the resulting spectral changes are shown in Figure 2a (red spectrum). We observe an increase in the oxygen-derived valence band intensity and a shift to higher binding energy. The spectral shift can be associated with a reduction of trapped charge, where activated oxygen species passivate the surface vacancies.¹⁶ This result is further corroborated by the fact that the number of equilibrium surface and bulk oxygen defects in ZnO is a function of the environmental oxygen partial pressure and temperature.¹⁷ The variations in surface stoichiometry produced from facile formation of oxygen vacancies highlights the sensitivity of the mea-

surement, which would not be found from an ensemble measurement.

It was also possible to generate oxygen vacancies by exposing the NWs to substantially higher 200 nm flux than that used for data collection. Figure 2b displays a reduction of valence band intensity and a spectral shift to lower binding energies with increasing light exposure. This result was due to desorption of oxygen by photogenerated holes that migrated to the surface along the potential slope created by band bending.¹⁸ As shown in Figure 2a,b, the high sensitivity of the nanowire surface and work function to molecular adsorption processes makes them ideal candidates to study other adsorption signatures such as those generated from covalently bound dipolar organic molecules.

Adsorption of polar organic molecules on semiconductor surfaces has been shown to induce significant changes in the electrostatic potential and in turn, electron affinity (χ) and work function (Φ). To date quantifying the effect that SAMs exert on various physical properties has been challenging, as electrical contacts to passivated surfaces often degrade the organic monolayer. Photoelectron spectroscopy on individual NWs is a salient method for correlating the interaction between adsorbed dipolar molecules and NW electronic structure because of the surface sensitivity of the technique.

SAMs of various phosphonic acid (PA) derivatives were chosen as a platform to study changes in Φ because PAs are strong binders to metal oxides¹⁹ and have been shown to have a pronounced effect on the electronic properties of ZnO thin films.²⁰ Additionally, the high density of surface binding sites in ZnO provided excellent accessibility for PA-based SAMs to target the surface and form up to three bonds at the interface,²¹ exerting a strong molecule–surface coupling.

Figure 3a demonstrates spectra taken before (blue curve) and after functionalization (red curve) with benzyl phosphonic acid (BPA), an electron-donating SAM with net dipole moment pointing toward the surface. The spectrum after functionalization with BPA was shifted by 0.4 eV to lower binding energy. To test whether the effect of the adsorbed molecule could be reversed, the substrate was annealed in situ at 300 °C for 2 min and resulted in a shift back toward its original state (green curve). That it does not fully recover back to its initial binding energy may be due to residual hydrocarbon left from the thermal desorption of the SAM. In all cases described below, partial or total recovery of the initial “clean” state was realized after annealing. To guarantee the observed shifts were from the functionalization and not a shift in the orientation of the NWs, a control experiment was run where the NWs were immersed in the solvent in the absence of the ligand under the same conditions and tested. No significant difference in the spectrum was observed from processing, indicating the orientation of the NW to the de-

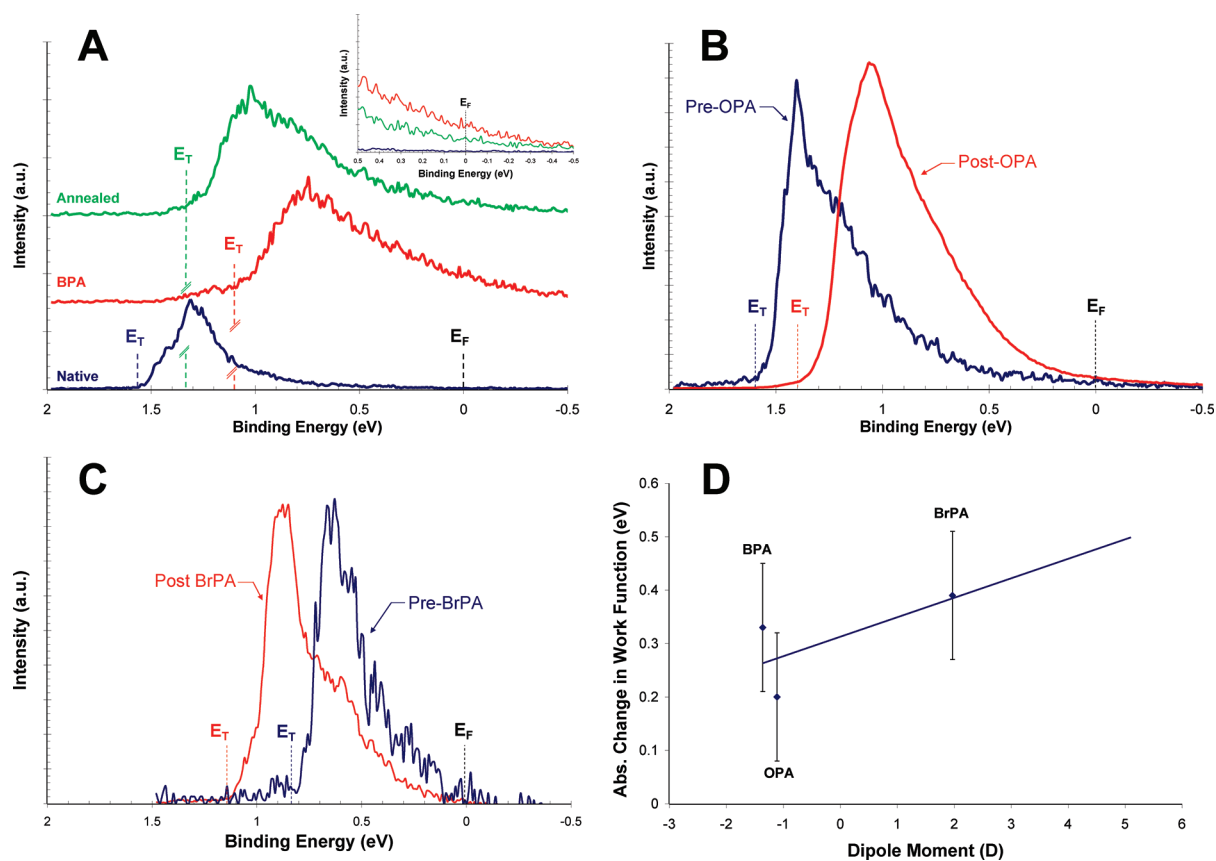


Figure 3. (a) Photoemission spectra taken on native NW (blue spectrum), after functionalization with benzyl phosphonic acid (red spectrum), and post annealing NW in situ (green spectrum). The spectra have been offset for clarity. The inset is a magnified view of the Fermi level (E_F) for all three plots. (b) Photoemission spectra taken on native NW (blue spectrum), and after functionalization with *n*-octylphosphonic acid (red spectrum). The electron emission thresholds (E_T) for each are color labeled by dashed lines. (c) Photoemission spectra taken on native NW (blue spectrum), and after functionalization with 4-bromophenylphosphonic acid (red spectrum). The electron emission thresholds (E_T) for each are color labeled by dashed lines. (d) Plot of changes to ZnO work functions ($\Delta\Phi$) using SAMs with various net dipole moments. As the strength of the net dipole moment increases, the work function increases linearly. The trend line represents the output from eq 1 and shows good agreement with the experimental results.

tor remained unchanged. Figure 3b demonstrates a representative spectrum taken before (navy curve) and after functionalization (red curve) with *n*-octyl phosphonic acid (OPA). OPA is also an electron-donor phosphonic acid but is an aliphatic system, and was selected to contrast the aryl-phosphonic acid SAMs used. Alkylphosphonic acids have been shown to have higher molecular packing densities and exert better coverage than aromatic SAMs. For the native nanowire, E_T was identified in Figure 3b at 1.6 eV. After functionalization, E_T was spectroscopically shifted by 0.2 eV to 1.40 eV, indicating a smaller change in the effective work function than for BPA. The results of the nanowires functionalized with BPA and OPA were consistent with the results of other electron donors at the surface (oxygen vacancies), where a shift of the valence edge toward the Fermi level was detected.

To gauge if the dipolar effect could be shifted in the reverse direction using oppositely charged dipoles, an electron-accepting phosphonic acid, 4-bromophenyl phosphonic acid (4-BrPA), with similar dipole strength but pointing away from the surface was grafted onto the nanowire. Figure 3c shows a representative spec-

trum of a nanowire passivated with BrPA. The spectra and E_T for a clean nanowire (red curve) were shifted by 0.4 eV after passivation (navy curve), indicating a large change in Φ . For the number of samples treated with 4-BrPA, the average shift of the emission threshold was 0.4 eV. The spectroscopic results found with 4-BrPA were qualitatively consistent with those found for dry oxygen (surface acceptors), whereby a shift of the valence edge away from the Fermi level was detected upon absorption.

The changes in Φ due to adsorption of polar SAMs stem from several molecular contributions. The first is a constant charge transfer effect from the phosphonic acid binding groups to the semiconductor surface.²² The next is the effect of the electronegativity of the headgroup of the molecule that contains the functional element that determines the net dipole moment, and the direction in which it points (to or from the surface). In addition to the electrostatic effect exerted from the dipoles, the polar SAMs may have also changed the net surface charge and depletion width by modulating the distribution of surface states. Changes in Φ also were studied by contrasting an alkylphosphonic acid with the

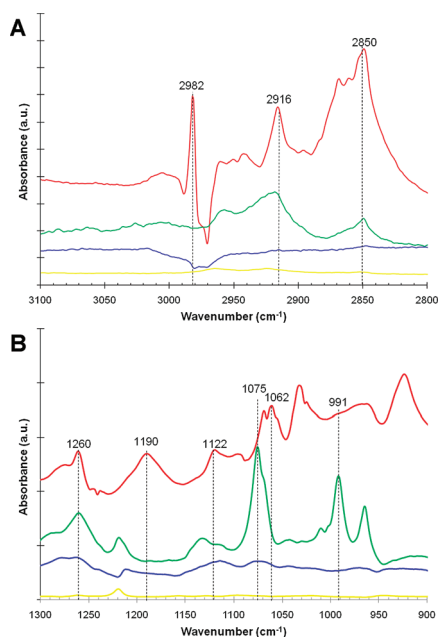


Figure 4. (A) Fourier transform infrared spectra in attenuated total reflectance (FTIR-ATR) mode of ZnO NWs grafted with phosphonic acid-based self-assembled monolayers (SAMs): methylene stretching vibration bands (2915 and 2848 cm^{-1}) of ZnO NWs functionalized with BrPA (red spectra), BPA (green curve), OPA (blue curve), and unfunctionalized NWs (yellow curve). The spectra have been offset for clarity. (B) Magnified view of FTIR-ATR spectra showing changes in the number and frequencies of the P=O and P–O stretching bands (990–1010, 1130, 1260–1300 cm^{-1}) for NWs functionalized with various SAMs: ZnO NWs functionalized with BrPA (red), BPA (green), OPA (blue), and unfunctionalized NWs (yellow).

aryl systems, though the binding results were not as conclusive. Figure 3d compares the calculated dipole moments of the SAMs used and the average shift in the work function. The dipole moments were calculated with Spartan software (Wave function Inc.) in an equilibrium geometry in the ground state using the Hartree–Fock method and 3-21G* basis set.

Fourier transform infrared spectra in attenuated reflectance mode (FTIR-ATR, Thermo Mattson Infinity Gold) of the functionalized NWs provided insight into the binding mode(s) of the SAMs to the NW surface (Figure 4). Strong binding between the aryl SAMs (BPA

and BrPA) and the nanowire surface was found, as evidenced by the methylene asymmetric ($\nu_s(\text{CH}_2)$) and symmetric ($\nu_s(\text{CH}_2)$) stretching absorptions at 2918 and 2850 cm^{-1} , respectively. The P–O stretching region (Figure 4a) also demonstrated considerable changes in the number and frequencies of the P=O and P–O stretching bands (990–1010, 1130, 1260–1300 cm^{-1}). Also apparent is the disappearance of the peaks at 950 cm^{-1} , which was indicative that the majority of the ligand is bound to the surface in a tridentate form. It should be noted however that since the ranges for the different P–O stretching peaks greatly overlap and depend on the degree of metal-binding, a definitive assignment of these bands was difficult. For the alkyl system (OPA), the methylene stretching absorptions showed the binding was much less pronounced. The changes to the P–O stretching region also showed a relatively weak interaction, which corroborates the magnitude of the small spectroscopic shift.

CONCLUSION

In summary, we have quantitatively measured the work function and location of the Fermi level of single hydrothermally grown ZnO NWs using low energy photoelectron spectroscopy. Systematic surface treatments were conducted to reveal the impact of environmental adsorbates on the work function as well as allow estimation of their effects on the surface densities of states. Future work involves studies on the effect of surface states as a function of diameter.²³ The technique was then extended to assess the interactions between various dipolar phosphonic acid-based SAMs and the NW work function. The molecular control imparted by the SAMs enables a versatile approach to tune the properties and performance of ZnO NWs and should have broad implications in photovoltaic²⁴ and optoelectronic devices where interface engineering is needed to enhance efficiencies and functionalities. The novel optical diagnostic technique also lends itself to the study of other nanomaterials and offers sufficient versatility and speed to probe spatially localized doping regions along an individual 1-D nanostructure.

METHODS

ZnO NWs were prepared using a solution-based synthesis where NW arrays were hydrothermally grown from preformed “c-axis” textured nanocrystals²⁵ prepared on a Si substrate. The seed-coated substrates were placed upside down for 36 h into an aqueous solution of 25 mM zinc nitrate hexahydrate ($\text{Zn}(\text{NO}_3)_2 \cdot 6\text{H}_2\text{O}$), 25 mM hexamethylenetetramine, and 7 mM branched low-molecular weight polyethylenimine (PEI) at 88 °C. After growth, the arrays were rinsed thoroughly with deionized water, baked in vacuum at 150 °C for 1 h and cleaned with UV/ozone for 10 min. The NWs have diameters ranging from 35 to 300 nm and variable lengths from 6 to 12 μm . The growth substrate was then immersed in VLSI-grade 2-propanol and soni-

cated for 10 s. The solution was then drop-cast onto a lithographically patterned Si wafer that contained etched-through slots (ca. 20–30 μm wide \times 1 mm length). The Si wafers were also lithographically dressed with metal alphanumeric characters adjacent to the slots to help identify the NW locations in an ultrahigh vacuum (UHV) chamber. Individual NWs of various diameters (90–200 nm) were picked up and aligned by nanomanipulation (Zyvx S100), and welded to the substrate by electron-beam-induced deposition of platinum. The metal welding prevented the nanowires from moving or rolling and since the nanowires were of relatively thick diameter (>90 nm) they did not bend and change the orientation of the nanowire to the de-

tector. Each NW was typically well separated from another (~ 50 μm), and hanging over the slit by at least 4–5 μm .

The layer of organic molecules with a net dipole moment perpendicular to the surface was grafted onto individual NWs using the tethering by aggregation and growth (T-BAG) method.²⁶ Prior to functionalization, the NW and Si substrate on which they rested were washed with deionized water and ethanol, dried with nitrogen, cleaned with oxygen plasma (50 W, 35 sccm, 100 s) and submerged into 50 μM solutions of benzylphosphonic acid (Alfa Aesar), *n*-octylphosphonic acid (Alfa Aesar), or (4-bromophenyl)phosphonic acid (Aldrich) prepared in neat tetrahydrofuran (THF) at 40 °C and let saturate for approximately 9–10 h. Slightly tempering the solvent above room temperature provided some thermal energy to assist the binding of the capping ligand to the surface as well as aid in evaporating the solvent. Once the solvent had evaporated, the substrate was placed in an oven at 80 °C overnight to covalently bond the molecules. The samples were then washed thoroughly with THF, washed again with a solution of water/THF/triethylamine (10:3:1) to remove nonspecific molecules that were not strongly chemisorbed to the NW surface, and washed again with THF and water. The functionalized NWs were then immediately loaded into the UHV system and interrogated the next day after the system had been fully pumped down. A control experiment was performed in the absence of the ligand and no significant differences in the spectrum were found, supporting that the NW maintained its orientation during processing.

Acknowledgment. The work is supported by grants to S.C. from the American Heart Association and the U.S. National Science Foundation. The authors would like to thank B. Long and C. G. Willson of the chemistry department at the University of Texas for providing assistance with the Spartan software and dipole moment calculations. The authors would also like thank J. A. Bardecker and A. Afzali of the I.B.M.—T.J. Watson Research Center for insightful discussions.

REFERENCES AND NOTES

- Huang, M. H.; Mao, S.; Feick, H.; Yan, H.; Wu, H.; Kind, H.; Weber, E.; Russo, R.; Yang, P. Room-Temperature Ultraviolet Nanowire Nanolasers. *Science* **2001**, *292*, 1897–1899.
- Law, M.; Greene, L. E.; Goldberger, J.; Johnson, J. C.; Saykally, R. J.; Yang, P. Nanowire Dye-Sensitized Solar Cells. *Nat. Mater.* **2005**, *4*, 455–459.
- Kind, H.; Yan, H. Q.; Messer, B.; Law, M.; Yang, P. Nanowire UV Photodetector and Optical Switches. *Adv. Mater.* **2002**, *14*, 158–160.
- Soci, C.; Zhang, A.; Xiang, B.; Dayeh, S. A.; Aplin, D. P. R.; Park, J.; Bao, X. Y.; Lo, Y. H.; Wang, D. ZnO Nanowire UV Photodetectors with High Internal Gain. *Nano Lett.* **2007**, *7*, 1003–1009.
- Ju, S. Y.; Facchetti, A.; Xuan, Y.; Liu, J.; Ishikawa, F.; Ye, P. D.; Zhou, C. W.; Marks, T. J.; Janes, D. B. Fabrication of Fully Transparent Nanowire Transistors for Transparent and Flexible Electronics. *Nat. Nanotechnol.* **2007**, *2*, 378–384.
- Sfeir, M. Y.; Beetz, T.; Wang, F.; Huang, L.; Huang, X.; Huang, M.; Hone, J.; O'Brien, S.; Misewich, J.; Heinz, T. F.; *et al.* Probing Electronic Transitions in Individual Carbon Nanotubes by Rayleigh Scattering. *Science* **2006**, *312*, 554–556.
- Bachilo, S. M.; Strano, M. S.; Kittrell, C.; Hauge, R. H.; Smalley, R. E.; Weisman, R. B. Structure-Assigned Optical Spectra of Single-Walled Carbon Nanotubes. *Science* **2002**, *298*, 2361–2366.
- Vogel, E. M. Technology and Metrology of New Electronic Materials and Devices. *Nature Nanotechnol.* **2007**, *2*, 25–32.
- Haight, R.; Sirinakis, G.; Reuter, M. Photoelectron Spectroscopy of Individual Nanowires of Si and Ge. *Appl. Phys. Lett.* **2007**, *91*, 233116.
- Hannon, J. B.; Afzali, A.; Klinke, C.; Avouris, P. Selective Placement of Carbon Nanotubes on Metal-Oxide Surfaces. *Langmuir* **2005**, *21*, 8569–8571.
- Klinke, C.; Hannon, J. B.; Afzali, A.; Avouris, P. Field-Effect Transistors Assembled from Functionalized Carbon Nanotubes. *Nano Lett.* **2006**, *6*, 906–910.
- Lim, D.; Haight, R. *In Situ* Photovoltage Measurements Using Femtosecond Pump-Probe Photoelectron Spectroscopy and Its Application to Metal–HfO₂–Si Structures. *J. Vac. Sci. Technol., A* **2005**, *23*, 1698.
- Long, J. P.; Sadeghi, H. R.; Rife, J. C.; Kabler, M. N. Surface Space-Charge Dynamics and Surface Recombination on Silicon (111) Surfaces Measured with Combined Laser and Synchrotron Radiation. *Phys. Rev. Lett.* **1990**, *64*, 1158–1161.
- Bescocke, K.; Krahl-Urban, B.; Wagner, H. Dipole Moments Associated With Edge Atoms; A Comparative Study on Stepped Pt, Au, and W Surfaces. *Surf. Sci.* **1977**, *68*, 39–46.
- Seker, F.; Meeker, K.; Kuech, T. F.; Ellis, A. B. Surface Chemistry of Prototypical Bulk II–VI and III–V Semiconductors and Implications for Chemical Sensing. *Chem. Rev.* **2000**, *100*, 2505–2536.
- Jacobi, K.; Zwicker, G.; Gutmann, A. Work Function, Electron Affinity, and Band Bending of Zinc Oxide Surfaces. *Surf. Sci.* **1984**, *141*, 109–125.
- Takahashi, Y.; Kanamori, M.; Kondoh, A.; Minoura, H.; Ohya, Y. Photoconductivity of Ultrathin Zinc Oxide Films. *Jpn. J. Appl. Phys.* **1994**, *33*, 6611–6615.
- Kolmakov, A.; Moskovits, M. Chemical Sensing and Catalysis by One-Dimensional Metal–Oxide Nanostructures. *Annu. Rev. Mater. Res.* **2004**, *34*, 151–80.
- Gao, W.; Dickinson, L.; Grozinger, C.; Morin, F. G.; Reven, L. Self-Assembled Monolayers of Alkylphosphonic Acids on Metal Oxides. *Langmuir* **1996**, *12*, 6429–6435.
- Salomon, A.; Berkovich, D.; Cahen, D. Molecular Modification of an Ionic Semiconductor–Metal Interface: ZnO/Molecule/Au Diodes. *Appl. Phys. Lett.* **2004**, *82*, 1051–1053.
- Mutin, P. H.; Guerrero, G.; Vioux, A. Hybrid Materials from Organophosphorus Coupling Molecules. *J. Mater. Chem.* **2005**, *15*, 3761–3768.
- Cahen, D.; Hodes, G. Molecules and Electronic Materials. *Adv. Mater.* **2002**, *14*, 789–798.
- Chiou, J. W.; Kumar, K. P. K.; Jan, J. C.; Tsai, H. M.; Bao, C. W.; Pong, W. F.; Chien, F. Z.; Tsai, M.-H.; Hong, I.-H.; Klausner, R.; *et al.* Diameter Dependence of the Electronic Structure of ZnO Nanorods Determined by X-ray Absorption Spectroscopy and Scanning Photoelectron Microscopy. *Appl. Phys. Lett.* **2004**, *85*, 3220–3222.
- Monson, T. C.; Lloyd, M. T.; Olson, D. C.; Lee, Y. J.; Hsu, J. W. P. Photocurrent Enhancement in Polythiophene- and Alkanethiol-Modified ZnO Solar Cells. *Adv. Mater.* **2008**, *20*, 4755.
- Greene, L. E.; Law, M.; Tan, D. H.; Montano, M.; Goldberger, J.; Somorjai, G.; Yang, P. General Route to Vertical ZnO Nanowire Arrays Using Textured ZnO Seeds. *Nano Lett.* **2005**, *5*, 1231–1236.
- Hanson, E. L.; Schwartz, J.; Nickel, B.; Koch, N.; Danisman, M. F. Bonding Self-Assembled, Compact Organophosphonate Monolayers to the Native Oxide Surface of Silicon. *J. Am. Chem. Soc.* **2003**, *125*, 16074–16080.